O_3-N_2O correlations from the Atmospheric Chemistry Experiment: revisiting a diagnostic of transport and chemistry in the stratosphere

JOURNAL OF GEOPHYSICAL RESEARCH, VOL. 112, D19301, doi:10.1029/2006JD008281, 2007

O_3-N_2O correlations from the Atmospheric Chemistry Experiment: Revisiting a diagnostic of transport and chemistry in the stratosphere

Michaela I. Hegglin[1] and Theodore G. Shepherd[1]

Received 24 November 2006; revised 6 June 2007; accepted 26 June 2007; published 3 October 2007.

[1] Our knowledge of stratospheric O_3-N_2O correlations is extended, and their potential for model-measurement comparison assessed, using data from the Atmospheric Chemistry Experiment (ACE) satellite and the Canadian Middle Atmosphere Model (CMAM). ACE provides the first comprehensive data set for the investigation of interhemispheric, interseasonal, and height-resolved differences of the O_3-N_2O correlation structure. By subsampling the CMAM data, the representativeness of the ACE data is evaluated. In the middle stratosphere, where the correlations are not compact and therefore mainly reflect the data sampling, joint probability density functions provide a detailed picture of key aspects of transport and mixing, but also trace polar ozone loss. CMAM captures these important features, but exhibits a displacement of the tropical pipe into the Southern Hemisphere (SH). Below about 21 km, the ACE data generally confirm the compactness of the correlations, although chemical ozone loss tends to destroy the compactness during late winter/spring, especially in the SH. This allows a quantitative comparison of the correlation slopes in the lower and lowermost stratosphere (LMS), which exhibit distinct seasonal cycles that reveal the different balances between diabatic descent and horizontal mixing in these two regions in the Northern Hemisphere (NH), reconciling differences found in aircraft measurements, and the strong role of chemical ozone loss in the SH. The seasonal cycles are qualitatively well reproduced by CMAM, although their amplitude is too weak in the NH LMS. The correlation slopes allow a ''chemical'' definition of the LMS, which is found to vary substantially in vertical extent with season.

Citation: Hegglin, M. I., and T. G. Shepherd (2007), O_3-N_2O correlations from the Atmospheric Chemistry Experiment: Revisiting a diagnostic of transport and chemistry in the stratosphere, *J. Geophys. Res.*, *112*, D19301, doi:10.1029/2006JD008281.

1. Introduction

[2] Transport and mixing are important processes in the stratosphere, determining the spatial distribution of long-lived chemical species that affect the chemical and radiative balance of the region. The representation of transport and mixing in chemistry-climate models (CCMs) needs to be validated against observations in order to have confidence in the models and their predictions concerning climate change and the recovery of the ozone layer. A challenge in this respect is the limited number of measurements of long-lived species in the stratosphere, and their inhomogeneous sampling in space and time.

[3] Sufficiently long lived species exhibit compact correlations [*Plumb and Ko*, 1992], which eliminate day-to-day variations, providing an ''instant climatology,'' and mean that even limited measurements can provide a robust constraint on models [*Sankey and Shepherd*, 2003]. There has been much interest in the use of O_3-N_2O (or O_3-CH_4) correlations as a diagnostic of transport and chemistry in the stratosphere. Over most of the stratosphere ozone is, however, not particularly long lived and the alignment of ozone isopleths is completely different from that of long-lived species such as N_2O, which resemble the distribution of age of air (Figure 1). As a consequence, the O_3-N_2O correlations are far from being compact and attention has focused on the variations of the correlations with altitude, latitude, and season. *Proffitt et al.* [2003] suggested the use of O_3 and N_2O averages binned by potential temperature or altitude as a diagnostic for transport and chemistry in models. *Khosrawi et al.* [2004, 2006] applied this method to O_3 and N_2O measurements from the ILAS and ILAS-II satellites in order to derive their seasonal evolution at high latitudes.

[4] In the lower stratosphere (LS) and lowermost stratosphere (LMS), as well as during polar night, the photochemical lifetime of ozone increases up to one year and the O_3-N_2O relation is expected to be reasonably compact. Indeed, the slope of the O_3-N_2O correlation in the lower stratosphere has been used in a wide range of studies to trace chemical ozone loss in the polar regions [*Proffitt et al.*, 1989, 1990, 1993; *Michelsen et al.*, 1998; *Müller et al.*, 2001, 2003; *Tilmes et al.*, 2006], identify transport and

[1]Department of Physics, University of Toronto, Toronto, Ontario, Canada.

0148-0227/07/2006JD008281$09.00

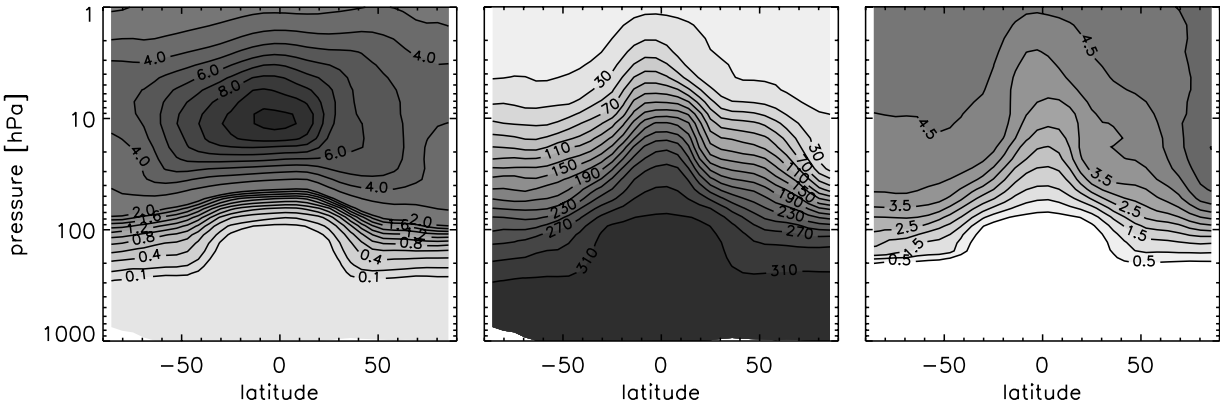

Figure 1. Zonal means of O_3 (ppmv), N_2O (ppbv), and age of air (year) obtained from the Canadian Middle Atmosphere Model (CMAM) for March 2000 from the simulation discussed in section 2.2. The well-known distributions of the two chemical tracers are the result of their particular source regions, their chemical lifetimes, and the effect of transport and mixing. Because of its relatively long lifetime, the N_2O distribution tends to resemble that of age of air. The O_3 distribution is clearly distinct from that of N_2O in the middle stratosphere, but tends to align with it in the lower stratosphere where the O_3 lifetime approaches one year (apart from polar spring).

mixing [*Waugh et al.*, 1997; *Bregman et al.*, 2000], and quantify the flux of ozone into the troposphere [*Murphy and Fahey*, 1994]. While satellite measurements usually lack accuracy in this region, ER-2 aircraft measurements at around 14–21 km altitude during the 1980s and 1990s provided a first insight into the seasonal and latitudinal dependencies of the O_3-N_2O relationship [*Strahan*, 1999; *Proffitt et al.*, 2003]. The observed equator-to-pole gradient and seasonal variations in the O_3-N_2O correlation slopes were interpreted in terms of a combination of stratospheric transport and mixing, and O_3 chemistry. Below ER-2 altitudes, aircraft measurements obtained during the SPURT campaign in the Northern Hemisphere LMS between 8 and 14 km identified also a distinct seasonal cycle in the O_3-N_2O correlation slopes, which however is different from that of the ER-2 measurements [*Hegglin et al.*, 2006]. No latitudinal dependencies were further identified during SPURT. The difference in behavior between the two altitude ranges was attributed to differences in the relative strength of transport and mixing within the tropically controlled transition region (as defined by *Rosenlof et al.* [1997]) and the diabatic descent of older air from the deep stratosphere. Yet these studies have mainly had to rely on aircraft or balloon measurements which, until recently, have represented the majority of accurate simultaneous measurements of multiple chemical species in the lower stratosphere. Such measurements yield a spatially and temporally incomplete picture of the O_3-N_2O relationship.

[5] The Atmospheric Chemistry Experiment Fourier Transform Spectrometer (ACE-FTS, hereafter referred to as ACE) on Canada's SciSat-1 satellite [*Bernath et al.*, 2005] has provided accurate measurements of numerous chemical species throughout the stratosphere since January 2004, with a high vertical resolution of down to 1 km reaching into the upper troposphere. The ACE measurements allow the seasonal, latitudinal, altitudinal, and interannual coverage of the aircraft measurements and previous satellite measurements to be extended. This makes the ACE measurements a potentially valuable database for the validation of transport and chemistry in CCMs in this region.

[6] The purpose of this paper is to examine the O_3-N_2O correlation structure in the stratosphere using ACE data, particularly its seasonal, latitudinal, and altitudinal dependences, and to investigate its value for the validation of CCMs. Because ACE is a solar occultation instrument, the geographical coverage is uneven and there is the potential of sampling biases. To assess those biases, fields from the Canadian Middle Atmosphere Model (CMAM), a comprehensive CCM, are used. By subsampling the CMAM data set according to the ACE sampling and comparing it with the full model fields, the representativeness of the ACE data in the context of a given diagnostic can be assessed. Having done so, the ACE data can then be compared with the CMAM to help validate the latter. We wish to emphasize the importance of assessing the robustness of diagnostics against sampling biases prior to a model-measurement comparison in order to test their validity and overall applicability.

[7] The paper is structured as follows. The ACE and CMAM data are described in section 2. In section 3, we examine the entire stratosphere from the tropopause up to the stratopause in tracer-tracer space, using O_3-N_2O scatterplots from ACE. We argue that where the O_3-N_2O correlations are not compact, the structure of the scatterplots mainly reflects the ACE sampling. In order to eliminate sampling biases the data has to be area-weighted, which leads us to the calculation of joint (two-dimensional) probability density functions (PDFs). The representativeness of the ACE data is then tested by checking the consistency between PDFs of full and subsampled CMAM fields, before we move on to the ACE-CMAM comparison. The use of joint PDFs is presented as an alternative diagnostic to the method suggested by *Proffitt et al.* [2003]. In section 4, we focus on the lower stratosphere, where the O_3-N_2O correlations are generally compact. The good spatial and temporal coverage of the ACE data, compared to aircraft data, allows a better characterization

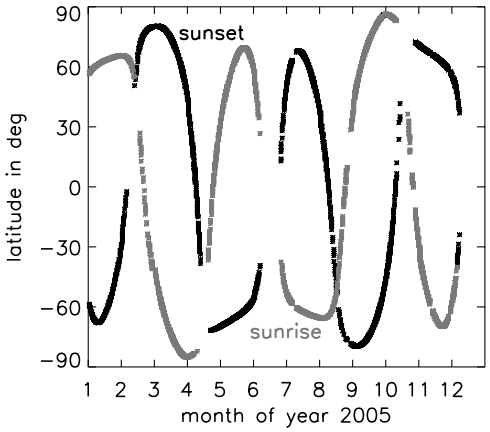

Figure 2. Time-dependent latitude scanning of the ACE satellite. The high-inclination (74°), circular, low-Earth orbit (650 km) of the ACE satellite provides global coverage with a focus on the Arctic polar region. During its orbits, ACE measures sequences of atmospheric absorption spectra during sunrise (shaded) and sunset (solid). The sampling pattern in other years is very similar to that in 2005.

of the seasonal, latitudinal, and vertical dependences of the correlations than has been hitherto possible. Again, we first compare the correlations derived from the full and the subsampled CMAM fields to test the robustness of the diagnostic, before we investigate the ability of CMAM to represent the observed features. We further analyze and interpret interhemispheric and seasonal differences in terms of the relative importance of transport and chemistry. The paper concludes with a summary and discussion in section 5.

2. Data Description

2.1. ACE Data

[8] In this study we use version 2.2 N_2O and version 2.2 updated O_3 data available between January 2004 and June 2006 from the ACE high-resolution infrared Fourier Transform Spectrometer (ACE-FTS, hereafter referred to as ACE) operating from 750 to 4400 cm^{-1} in solar occultation mode [*Bernath et al.*, 2005; *Boone et al.*, 2005]. The ACE satellite was launched into low Earth circular orbit (650 km) with high inclination (74°) on 12 August 2003. Figure 2 shows the resulting latitude scanning for the year 2005. 15 vertical profiles are taken during sunset and sunrise per day. Profiles with currently known retrieval biases are not included in the evaluations. ACE provides a seasonally varying coverage of the globe, with an emphasis on NH midlatitudes and the polar region. In Figure 3, the geographical locations of all profiles obtained during the chosen period are shown. In Table 1, the number of profiles per month, year, and latitude range are listed. ACE attains continuous latitudinal coverage from 85°S to 85°N when the measurements are accumulated over a season of a specific year. The selected data cover the altitude range between 8 and 50 km, i.e., the entire stratosphere. Over the course of a year, the altitude spacing for ACE measurements varies from approximately 1 to 6 km, depending on the beta angle of the satellite (the angle between the satellite orbit plane and the Earth-Sun vector). For this study, we use the retrieved data interpolated onto an equally spaced vertical grid of 1 km. The validation of the ACE version 2.2 data set (with ozone updates) is currently underway. This work includes comparisons to other satellite products, ground, balloon, and aircraft-based measurements. The version 1.0 ACE O_3 data have been compared with GOMOS satellite data [*Fussen et al.*, 2005] yielding good agreement between the two data sets with differences mostly lower than 10% between 15 and 45 km. A comparison with POAM III and SAGE III data yielded a similar result, however with a high bias above 40 km with differences up to 25% [*Walker et al.*, 2005]. Both studies reported also a low bias around the O_3 maximum. In the version 2.2 (with O_3 updates) used in this study, the low bias at lower altitudes had been corrected but the high bias at altitudes above 40 km still persists. This is under investigation as part of the validation work. The N_2O version 2.2 data were compared to MLS v2.2 data and showed very good agreement in an altitude range between 70 and 3 hPa with differences smaller than 5%. Above and below these heights the differences increase (to 15% at 100 hPa, and up to 20% above 3 hPa) (A. Lambert, personal communication, 2007). Equivalent latitude (kindly provided by Gloria Manney), used for the evaluations in section 4, has been calculated using Met Office data fields interpolated in space and time onto the location of the ACE vertical profiles.

2.2. CMAM Data

[9] The CMAM is an extension of the Canadian Centre for Climate Modelling and Analysis (CCCma) spectral General Circulation Model into the lower thermosphere up to 0.0006 hPa (around 100 km). The CMAM includes a comprehensive representation of the relevant physical and chemical processes in a fully interactive mode [*Beagley et al.*, 1997; *de Grandpré et al.*, 2000]. Model fields are calculated on a linear Gaussian transform grid with 32 × 64 grid points in the horizontal, corresponding to a spatial resolution of around 6° × 6°, and 71 vertical levels. The

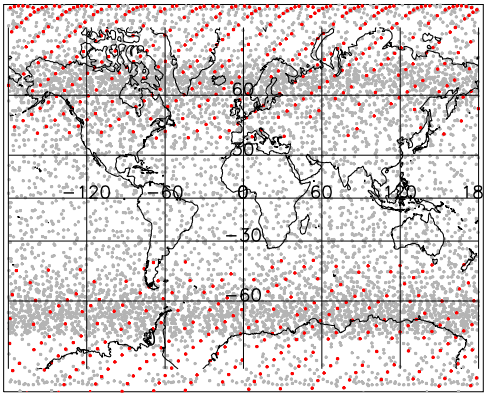

Figure 3. Geographical locations (gray dots) of all ACE retrievals taken between January 2004 and June 2006. Red dots show the sampling pattern for March 2005. The measurement density is highest in a latitude band between approximately 55° and 70° in both hemispheres. The lowest density is found in the tropics.

Table 1. Number of ACE Profiles Between January 2004 and June 2006 for Each Geographical Latitude Band, Month, and Year (2004/2005/2006)

	60–90°S	30–60°S	30–0°S	0–30°N	30–60°N	60–90°N
Jan	5/66/89	8/72/99	10/8/2	0/0/0	0/24/53	7/144/191
Feb	0/0/0	0/18/10	20/36/75	27/13/15	29/15/23	123/152/166
Mar	0/265/127	0/55/57	0/0/0	0/0/0	81/68/23	287/261/167
Apr	42/62/91	2/13/3	13/62/15	46/106/60	11/27/18	0/0/0
May	211/247/144	47/69/24	0/0/0	0/0/0	10/119/88	25/213/118
Jun	0/0/0	13/74/12	0/0/0	0/10/0	29/70/19	0/0/0
Jul	96/238/0	30/55/0	0/0/0	0/0/0	112/144/0	101/143/0
Aug	66/107/0	1/45/0	32/50/0	87/70/0	24/39/0	0/0/0
Sep	98/257/0	43/63/0	0/0/0	0/0/0	53/75/0	164/234/0
Oct	0/0/0	32/48/0	61/87/0	4/30/0	0/9/0	66/113/0
Nov	223/165/0	124/117/0	0/0/0	0/0/0	31/29/0	82/222/0
Dec	0/0/0	43/37/0	5/2/0	0/0/0	59/41/0	0/0/0

vertical resolution in the tropopause region is around 900 m, coarsening to around 2 km in the upper stratosphere. Data presented here correspond to 3-day sampling of instantaneous fields in the years 2000–2010 of a 150-year transient run from 1950 with CMAM version 8, using sea surface temperatures and sea ice distributions from an IPCC simulation with a coupled ocean-atmosphere model upon which the CMAM is based, and background aerosol forcing. Greenhouse gas surface concentrations evolve in time following the GHG scenario A1B (medium) of the IPCC Special Report on Emission Scenarios (SRES) [*Intergovernmental Panel on Climate Change*, 2000]. The surface halogens are prescribed according to the Ab scenario given by *World Meteorological Organization* [2003].

[10] *Sankey and Shepherd* [2003] examined chemical correlations (including O_3-N_2O) in an earlier version of CMAM, version 7, which was also the version of CMAM used for the model intercomparison of *Austin et al.* [2003]. Compared to version 7, CMAM version 8 includes several improvements, two of which are particularly important in the present context. First, the vertical resolution was increased, from 50 to 71 levels (over the same altitude range), and the vertical diffusivity K_{zz} decreased from 1 m^2 s^{-1} to 0.1 m^2 s^{-1}. The latter value is more realistic, and its use has eliminated some deleterious effects of the higher value of K_{zz} on model transport which were evident in the summer stratosphere (where other transport processes are less important): the vertical profiles of long-lived tracers are now much more realistic (S. Melo, personal communication, 2005), and summertime total ozone anomalies now persist rather than decaying prematurely [*Tegtmeier and Shepherd*, 2007]. The second important improvement is that a significant warm bias in the Arctic lower stratosphere during winter and spring (evident in the work by *Austin et al.* [2003]) has been eliminated. This warm bias led to the Arctic vortex being much too active and leaky [*Sankey and Shepherd*, 2003]. The improvement is attributed to a reduction in the critical inverse Froude number used to define wave breaking in the orographic gravity wave drag parameterization (following independent work by S. Webster and B. Boville (personal communication, 2004)).

[11] A detailed comparison of CMAM version 8 (run over 1960–2004 with observed sea surface temperatures and volcanic aerosol forcing) with observations is provided as part of the model intercomparison of *Eyring et al.* [2006]. This comparison shows that CMAM version 8 generally has quite reasonable transport properties, although the age of air tends to be a little too young and the mixing barriers (seen in latitudinal gradients of long-lived tracers) a little too

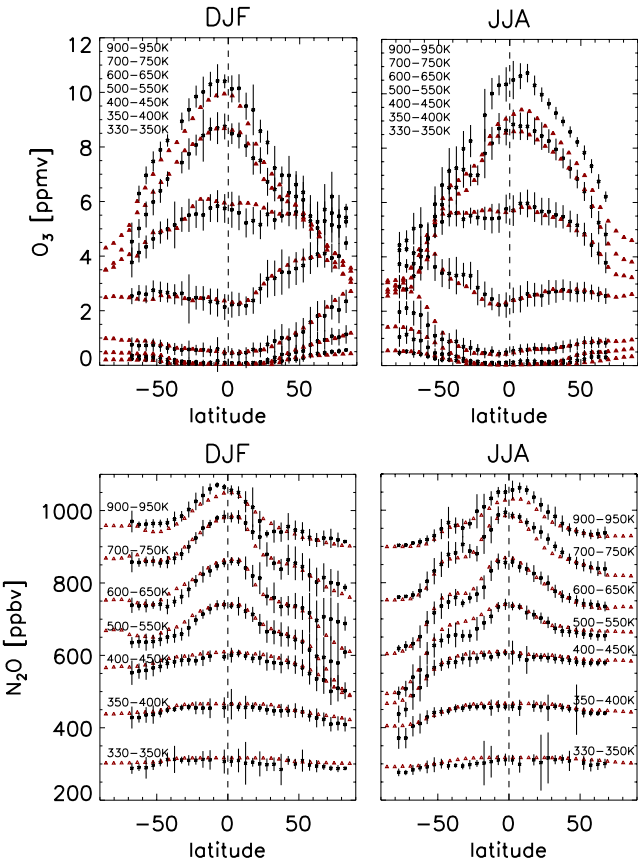

Figure 4. Latitudinal profiles of mean O_3 and N_2O mixing ratios from CMAM (red triangles) and ACE (black asterisks) for the solstice seasons as functions of potential temperature range (annotated in black). Black bars indicate the standard deviations ($\pm 1\sigma$) for the ACE data. N_2O profiles are offset by 150, 300, 450, 600, 750, and 900 ppbv, respectively, except the lowest level.

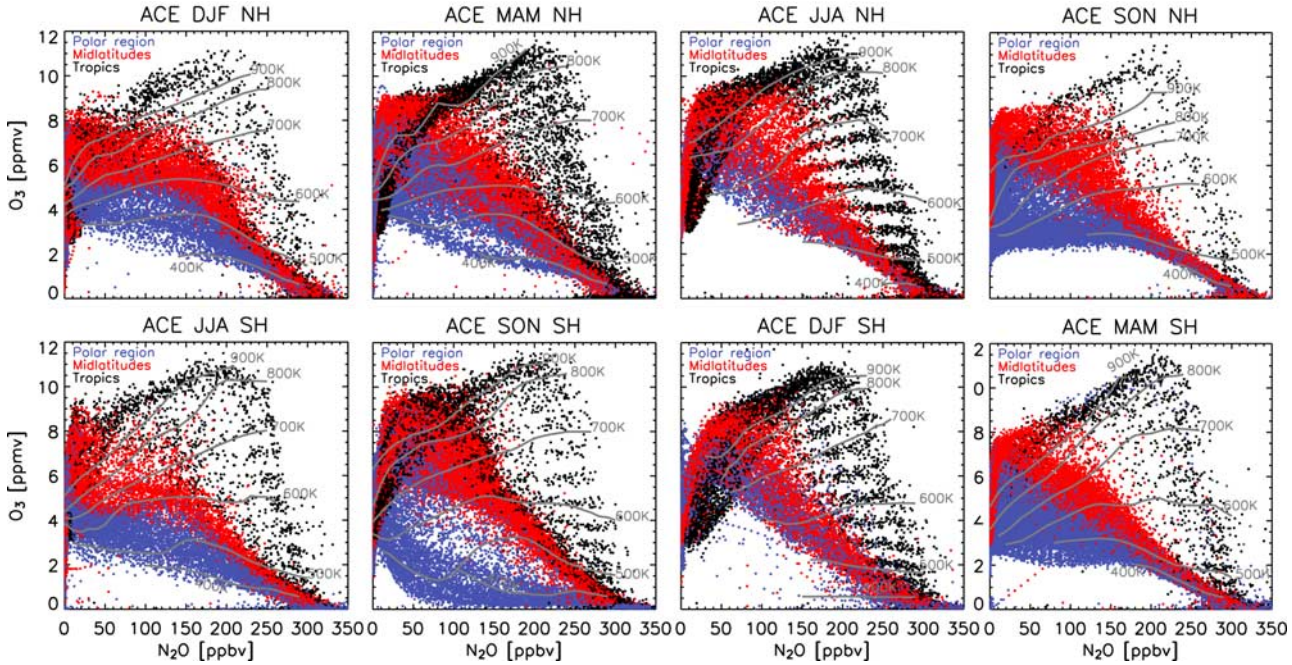

Figure 5. O_3-N_2O scatter plots from ACE in the NH and SH for each season (from left to right: winter, spring, summer, and autumn). Color coding classifies data according to their equivalent latitude into tropics (black), midlatitudes (red), and polar region (blue). Gray lines indicate surfaces of potential temperature, in K. The striations seen in some of the panels result from the finite vertical resolution of the ACE measurements.

weak. However, although the mean temperature bias in the Arctic winter/spring has been eliminated, CMAM still fails to simulate the coldest winters with severe Arctic ozone loss, and minimum Arctic springtime ozone values are systematically too high [*Eyring et al.*, 2007].

[12] Since the CMAM will be used in this study to investigate sampling issues of the ACE measurements, we provide an example to confirm that the model provides a reasonable representation of the relevant tracer distributions. To this end, Figure 4 shows latitudinal profiles of O_3 and N_2O from both ACE and CMAM for the solstice seasons, as functions of potential temperature range. (Note that the N_2O profiles are offset in the vertical for clarity.) The CMAM profiles are generally in excellent agreement with the ACE profiles, with the exception of O_3 at the highest potential temperature levels in summer. As mentioned above, there are some concerns about the quality of the ACE O_3 retrievals at these altitudes [*Walker et al.*, 2005]. However, unpublished comparisons with CMAM run in data assimilation mode, with temperatures constrained by observations, show better agreement with the ACE measurements. This likely results from the removal of an apparent upper stratospheric warm bias in the free-running CMAM, thereby increasing O_3 values, and increases the confidence in the ACE O_3 product.

[13] We will assess the representativeness of the ACE data in the context of a given diagnostic by subsampling the CMAM data set according to the ACE sampling, and comparing it with the full model fields. The subsampled CMAM data fields were produced by interpolation of the full O_3 and N_2O CMAM fields onto the location of each ACE profile at a given time.

3. The Stratosphere in O_3-N_2O Space

3.1. O_3-N_2O Scatterplots and Their Limitations

[14] A widely used approach to identify dynamical features or anomalies in chemical processing of air from tracer data is to examine tracer-tracer scatterplots [*Sankey and Shepherd*, 2003, and references therein]. The O_3-N_2O relationship in particular has been widely used from the late 1980s onward for this purpose [*Proffitt et al.*, 2003, and references therein].

[15] Figure 5 shows the ACE O_3-N_2O scatterplots for the full stratospheric altitude range up to 50 km, for all seasons and both hemispheres, colored according to their equivalent latitude. The individual panels include the data sampled over the whole observation period during the corresponding season. N_2O can be regarded roughly as a measure of age of air, with lower values corresponding to older ages (see Figure 1). Vertical profiles in the stratosphere exhibit an ozone maximum and the corresponding O_3-N_2O points form a boomerang shape, with a negative O_3-N_2O correlation below the ozone maximum and a positive correlation above. The ozone maximum takes higher values and occurs at higher N_2O values in the tropics than in the extratropics, so the boomerang shapes slump down and to the left as one moves to higher latitudes. This results in the fan-shaped structure to the correlation pattern evident in all the panels of Figure 5 [cf. *Proffitt et al.*, 2003].

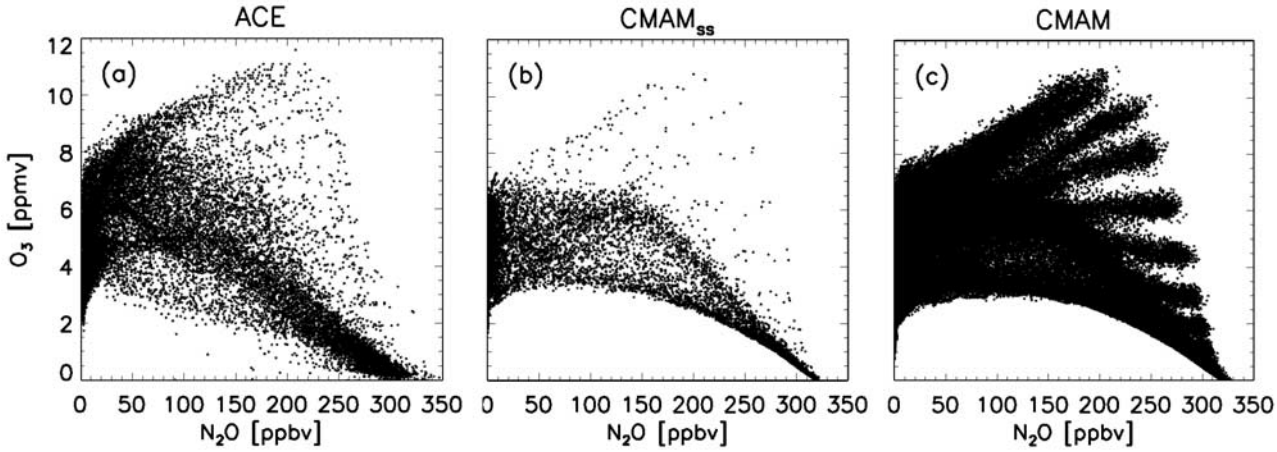

Figure 6. O_3-N_2O scatterplots (a) for ACE NH winter months (DJF) obtained in 2004/2005, (b) for CMAM data subsampled according to the ACE measurement locations, and (c) for the full CMAM fields in the NH over the same time period. The striations result from the finite vertical resolution of the CMAM data.

[16] In all seasons it is seen that over most of the stratosphere, the O_3-N_2O correlations are not compact and thus limited measurements such as balloon soundings [*Müller et al.*, 2003] or shuttle measurements [e.g., *Michelsen et al.*, 1998] might only sample a part of the overall distribution, with this part being crucially dependent on the actual dynamical state of the atmosphere. Only in the lower stratosphere, below approximately 21 km, do the correlations become more compact, and even then only outside of the tropics. A distinct polar branch is suggested in the SH winter as the vortex creates an isolated air mass [cf. *Sankey and Shepherd*, 2003, Figure 15]. The ACE data further suggest that the dynamical isolation continues in spring and the ozone values are depressed further (and lose compactness) because of chemical ozone loss. There is some indication of these processes in the NH winter and spring but to a much lesser extent.

[17] In the middle stratosphere, although the correlations are not compact, there are hints of clustering, i.e., O_3-N_2O pairs which apparently are measured more frequently, of tropical (e.g., MAM SH, JJA SH) and midlatitude (e.g., SON SH and DJF NH) points. Because of the limited sampling from ACE, however, it is not clear whether this clustering is real or is an artifact of the sampling. To address this issue we turn to CMAM, which provides a complete sampling in space and time. Figure 6b shows the CMAM data for DJF NH subsampled according to the ACE retrieval locations and times, which thus may be directly compared with the ACE scatterplot (Figure 6a). The distributions of the ACE and the subsampled CMAM data match well, and indeed the clustering is reproduced in the CMAM subsample. However, when the CMAM data are plotted with complete sampling in time and space for the winter months, as shown in Figure 6c, the distribution appears to be continuous and the qualitative impression of the clustering is lost. Scatterplots therefore reflect more the sampling rather than the real distribution of O_3-N_2O pairs. This is because the O_3-N_2O correlation is not compact; for a compact tracer-tracer correlation, sampling would not matter [*Sankey and Shepherd*, 2003].

3.2. Joint Probability Density Functions

[18] A way to reveal true clustering and thus allow a quantitative comparison with models is to weight the data according to their sampling. This is done by calculation of equal-area probability density functions (PDFs). For this purpose we mainly followed the suggestions of *Sparling* [2000]. The ACE and the subsampled CMAM data fields are unevenly sampled and in order to obtain near-global coverage and better statistics, the data were accumulated over each season (DJF, MAM, JJA, and SON) and the 2.5 years of the considered observation period. We calculate normalized PDFs for every 10° latitude band for O_3-N_2O bins with widths of 0.5 ppmv and 10 ppbv, respectively, weight the PDFs according to their area (the interpolated ACE data have equal vertical spacing), and add them up to create one normalized PDF for each hemisphere. The full CMAM fields for each season are accumulated over the same time period of 2.5 years, interpolated vertically, and then weighted by height and thinned in order to weight the points according to the area they represent. The full CMAM PDFs for both hemispheres are finally calculated for O_3-N_2O bins with widths of 0.25 ppmv and 5 ppbv, respectively.

3.3. Testing the ACE Sampling

[19] In order to test the representativeness of the ACE sampling and the robustness of the diagnostic, the seasonal PDFs of the full CMAM fields are compared to those of the subsampled CMAM fields. If the PDFs yield the same result we can have some confidence in the representativeness of the sampling and the robustness of the diagnostic. Figure 7 shows the seasonal PDFs of the full CMAM fields in color, with the contours of the seasonal PDFs of the subsampled CMAM data overlaid in black. The contour lines of the subsampled CMAM data largely follow the PDF contours of the complete CMAM data sets. However, the subsam-

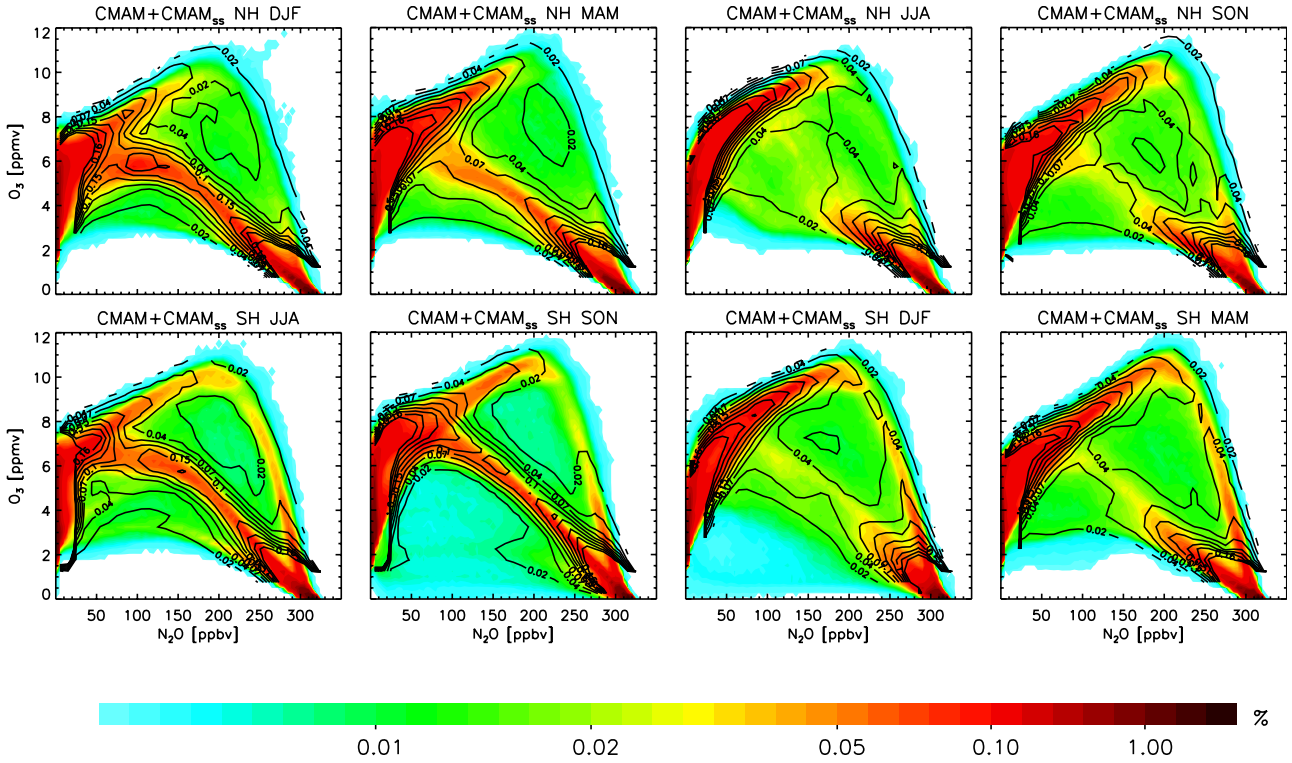

Figure 7. Probability density functions (PDFs) of O_3-N_2O pairs for CMAM (color coded) and CMAM subsampled according to the ACE sampling (black contour lines), expressed in relative units. The PDFs are shown for the NH and SH and for each season (from left to right: winter, spring, summer, and autumn). The subsampled CMAM PDF includes all data of a corresponding season obtained during the 2.5-year observation period. The CMAM PDF includes the full tracer fields over the same period. Both data sets are weighted using geographical latitude.

pling and the resulting use of larger data bins in the calculation of the subsampled PDFs leads to somewhat broader and less distinguishable features, as seen for the tropical pipe and the surf zone in the lower stratosphere. With this in mind we now move on to the direct comparison between the PDFs for the full CMAM fields and for ACE.

3.4. Model-Measurement Comparison

[20] Figure 8 shows again the seasonal PDFs of the full CMAM fields in color, but now it is the contours of the ACE PDFs that are overlaid in black. The full sampling of the CMAM allows a reliable estimation of the PDFs of O_3-N_2O pairs in the CMAM. High values of the PDF indicate regions with weak spatial gradients (generally implying homogenization by quasi-horizontal mixing), and low values regions with strong gradients (generally implying the presence of a mixing barrier) [cf. *Sparling*, 2000]. As pointed out by *Sparling* [2000], the use of PDFs is seen to obviate the need for equivalent latitude, as the structures emerge from the tracer fields themselves. This is a significant simplification for model-measurement comparison, where equivalent latitude is often not easily available.

[21] Figure 8 reveals in a succinct manner many key features of stratospheric transport and mixing. We first discuss the features in the CMAM PDF. The PDF maximum that slopes up and to the left through the middle of each panel represents the stratospheric surf zone, where strong horizontal mixing from breaking planetary waves leads to weak meridional gradients. In the NH, this feature is most prominent during winter and spring, and disintegrates during summer and autumn. In the SH, where the westerly regime is longer-lived and the "dynamical summertime" easterlies correspondingly shorter-lived, the reappearance of the PDF maximum is already evident in autumn. On either side of this PDF maximum are minima corresponding to the subtropical and polar vortex edges [cf. *Sankey and Shepherd*, 2003, Figure 10]. Tropical maxima, corresponding to the "tropical pipe," are evident in all seasons in the SH along the rightmost border of the PDFs, but only a tentative feature is seen in the NH during autumn. This indicates that the tropical pipe in CMAM is generally displaced into the SH. (If the tropical pipe was symmetric about the equator, one would see a maximum in both hemispheric PDFs [see, e.g., *Neu et al.*, 2003].) A polar vortex PDF maximum is apparent in SH winter. The PDF maximum sloping up and to the right along the leftmost border of the PDFs corresponds to points at and above the ozone maximum, where the vertical gradient of N_2O becomes weak; in contrast to the others, this feature is of chemical rather than dynamical origin. The extension of the PDF to very small ozone values seen in SH spring is likewise a chemical feature: the ozone hole.

[22] Now we focus on the contour lines in Figure 8 showing the PDFs from ACE. Where the data coverage (as

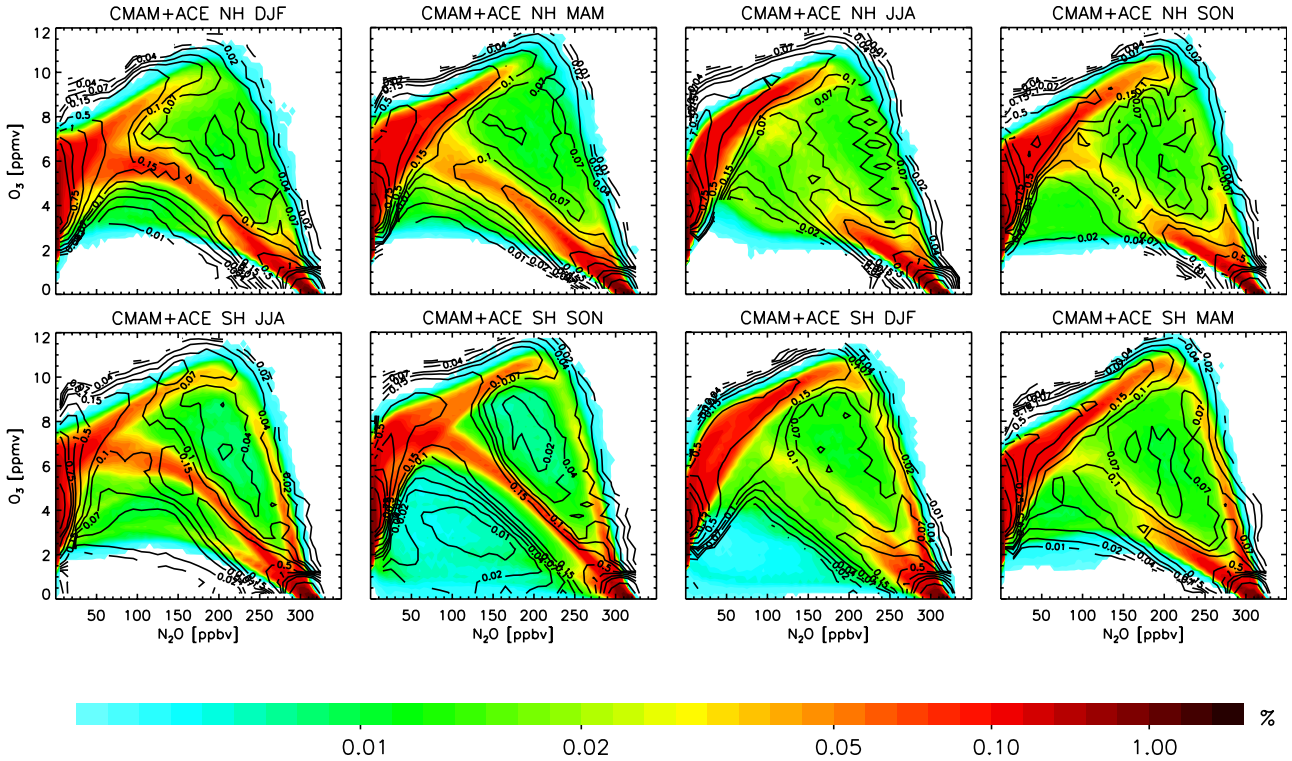

Figure 8. Same as Figure 7 but now the black contour lines are for the ACE data (over the entire season). Both data sets are weighted using geographical latitude.

evident in Figure 5) is poor, the resolution of the PDFs is somewhat noisy (e.g., NH SON). Nevertheless, the basic features seen in the CMAM PDFs are also, for the most part, evident in the ACE PDFs. In most seasons in the NH the correspondence is, in fact, quite remarkable. Two clear weaknesses of CMAM with respect to ACE are the persistence of low ozone values in the SH into DJF, a result of CMAM's too-late breakup of the SH vortex; and the fact that the "surf zone" maxima tend generally to lie to the right of the ACE features (particularly in SH JJA and SON), a result of CMAM's slightly too young age of air [*Eyring et al.*, 2006]. Another discrepancy between the two data sets exists at the highest altitude levels, where ACE O_3 and N_2O mixing ratios are up to 15% and 5% higher, respectively, than the mixing ratios from CMAM. As mentioned earlier with reference to Figure 4, the ozone discrepancy might reflect a problem with the ACE data [*Walker et al.*, 2005], and/or a warm bias in CMAM at these altitudes.

[23] The only major difference between the CMAM and ACE PDFs in Figure 8 is the lack of a tropical PDF maximum in CMAM in NH MAM and JJA along the right-most border of the PDFs, i.e., in CMAM the tropical pipe is shifted into the SH in all seasons. This discrepancy might be related to the absence of a QBO in this version of CMAM, as the QBO has been shown to have a distinct impact on the formation and characteristics of the subtropical mixing barrier [*O'Sullivan and Chen*, 1996]. Instead, CMAM exhibits weak easterly winds in the tropics year-round. In the SH, the tropical pipe is seen to exist in all seasons in both the CMAM and ACE data, though the feature is weak in the ACE data during JJA and SON. Since the subsampled CMAM PDFs in SH JJA and SON fail to reproduce the full strength of the tropical pipe PDF maxima (see Figure 7), this is likely due to a lack of representativeness of the ACE tropical sampling during these periods.

4. The Lower and Lowermost Stratosphere

[24] As mentioned in the introduction, the O_3-N_2O correlations are expected to become much more compact in the extratropical lower stratosphere, below approximately 21 km, and there are strongly reduced slopes at polar latitudes in the SH during winter and spring (see Figure 5). We can thus fit slopes to these correlations and examine their seasonal evolution. Aircraft measurements in the NH, from the ER-2 and during SPURT, have identified different seasonalities and latitudinal dependencies of the O_3-N_2O correlation slopes in the two altitude regions sampled by the different aircraft. In order to investigate these apparent discrepancies, we distinguish between what we will hereafter call the lower stratosphere (LS), corresponding to the altitude region sampled by the ER-2 measurements considered by *Proffitt et al.* [1990, 2003] and *Strahan* [1999], and what we will call the lowermost stratosphere (LMS), corresponding to altitudes closer to the tropopause considered by *Hegglin et al.* [2006]. The LS is here defined as the atmospheric region between 400 K and 500 K, and corresponds to altitudes between approximately 16 and 21 km. The LMS is here defined as the region between the tropopause and 400 K, and corresponds to altitudes between approximately 8–10 km and 16 km. Figure 9 is a sketch of the two regions. Highlighted are the two main processes influencing tracer distributions in the stratosphere, namely transport by the Brewer-Dobson circulation and isentropic

(quasi-horizontal) mixing. Also indicated is the edge of the tropical pipe, which acts as a barrier to horizontal mixing. Isentropic mixing is enhanced in the tropically controlled transition region [*Boering et al.*, 1996; *Volk et al.*, 1996; *Rosenlof et al.*, 1997], which lies between the tropical tropopause and an altitude of approximately 450 K. While the Brewer-Dobson circulation is mainly driven by the breaking of planetary-scale Rossby waves in the middle stratosphere, the mixing within the tropically controlled transition region is furthermore sustained by the breaking of synoptic-scale waves. The relative strength of the two processes and their seasonal evolution determine the distribution of tracers and with it the slope of tracer-tracer correlations, as shown for the LMS by *Hegglin et al.* [2006]. (In contrast, any direct mixing from the troposphere into the LMS is not expected to change the slope values, as it can be regarded as so-called "end-member" mixing [cf. *Waugh et al.*, 1997].) It is important that CCMs resolve these processes adequately and hence are capable of reproducing the seasonal change in LMS tracer composition since it influences the ozone chemistry [*Hegglin et al.*, 2006] and determines the radiative budget of this region.

[25] Figure 10 provides an example of two ACE O_3-N_2O scatterplots obtained during March 2004 and September 2005. Solid data points are sampled in the LMS, and shaded data points are sampled in the LS. The correlation slopes calculated for both regions evidently differ from each other. Because of the rise in tropopause height during summer and autumn, and the seasonal cycle in transport of O_3-rich and chemically aged air into the LMS, the O_3 and N_2O dynamic ranges in the LMS are smaller during autumn than during spring [*Logan*, 1999; *Hegglin et al.*, 2006].

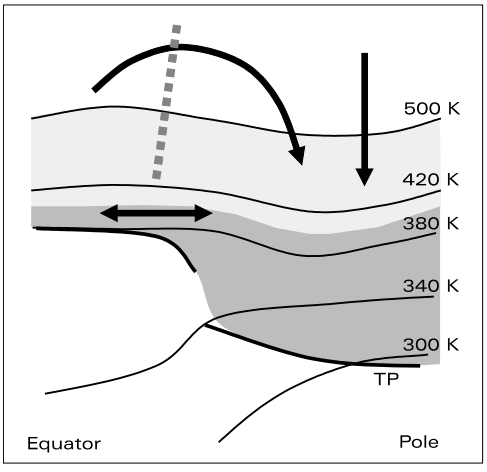

Figure 9. Sketch of the lower stratosphere (LS, between 400 K and 500 K) in light shading and the lowermost stratosphere (LMS, between the tropopause and 400 K) in dark shading, as defined in this study. The thick solid line denotes the tropopause, thin lines denote potential temperature surfaces, and the shaded dashed line denotes the subtropical mixing barrier. The thick arrows indicate the Brewer-Dobson circulation, while the double-headed arrow indicates rapid quasi-horizontal mixing in the tropically controlled transition region.

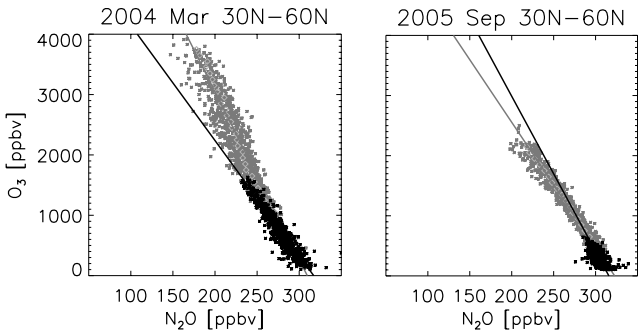

Figure 10. O_3-N_2O scatter plots from ACE for midlatitudes in (left) March 2004 and (right) September 2005. Shaded dots indicate measurements in the LS, and solid dots measurements in the LMS. Solid and shaded lines specify linear fits to the data points of the two corresponding regions. The data are classified according to their equivalent latitude.

4.1. O_3-N_2O Correlations

[26] For the calculation of the O_3-N_2O correlation slopes for ACE, the subsampled CMAM, and the full CMAM, the data are grouped by month and classified into four latitude bands, the polar regions (60–90°N and 60–90°S) and the midlatitudes (30–60°N and 30–60°S), to account for possible interhemispheric and latitudinal dependencies. We do not apply this diagnostic to the tropics because of the scarcity of the ACE measurements in this region. In order to reduce the scatter in the data caused by reversible transport processes and hence to increase the robustness of the calculated correlation slopes, all data have been classified according to their equivalent latitude. The selected data points are binned into equally spaced O_3 bins with a width of 0.1 ppmv, and for each bin the median N_2O mixing ratio is calculated in order to diminish the influence of outliers. The median was chosen rather than the mode, since the latter was not everywhere well defined. Correlation slopes are then calculated from a linear fit to the resulting O_3-N_2O pairs constrained by a tropospheric endpoint. The tropospheric O_3 value is chosen to be 100 ppbv, i.e., the value defining the chemical tropopause. For the LMS, the tropospheric N_2O value is determined by taking the mean of the tropospheric values of the respective data set and region. For the LS, the tropospheric endpoint has been chosen empirically at a lower N_2O value which takes into account the aging of the air masses (306 ppbv for ACE, 314 ppbv for CMAM). The higher value derived for the CMAM data set stems likely from a generally younger age of air than observations indicate. We emphasize that the calculation of the slopes is very sensitive to the choice of the endpoint N_2O values, and potential uncertainties in the latter may lead to errors in our correlation slope calculations. However, in order to gauge the quality of the fits and confirm the compactness of the correlations, we provide monthly scatter plots, the calculated linear fit, and the number of available data points in the different latitude bands for the LS in Figure 11, and for the LMS in Figure S1 in the auxiliary material.[1] The overall impression one gets from these

[1] Auxiliary material data sets are available at ftp://ftp.agu.org/apend/jd/2006jd008281. Other auxiliary material files are in the HTML.

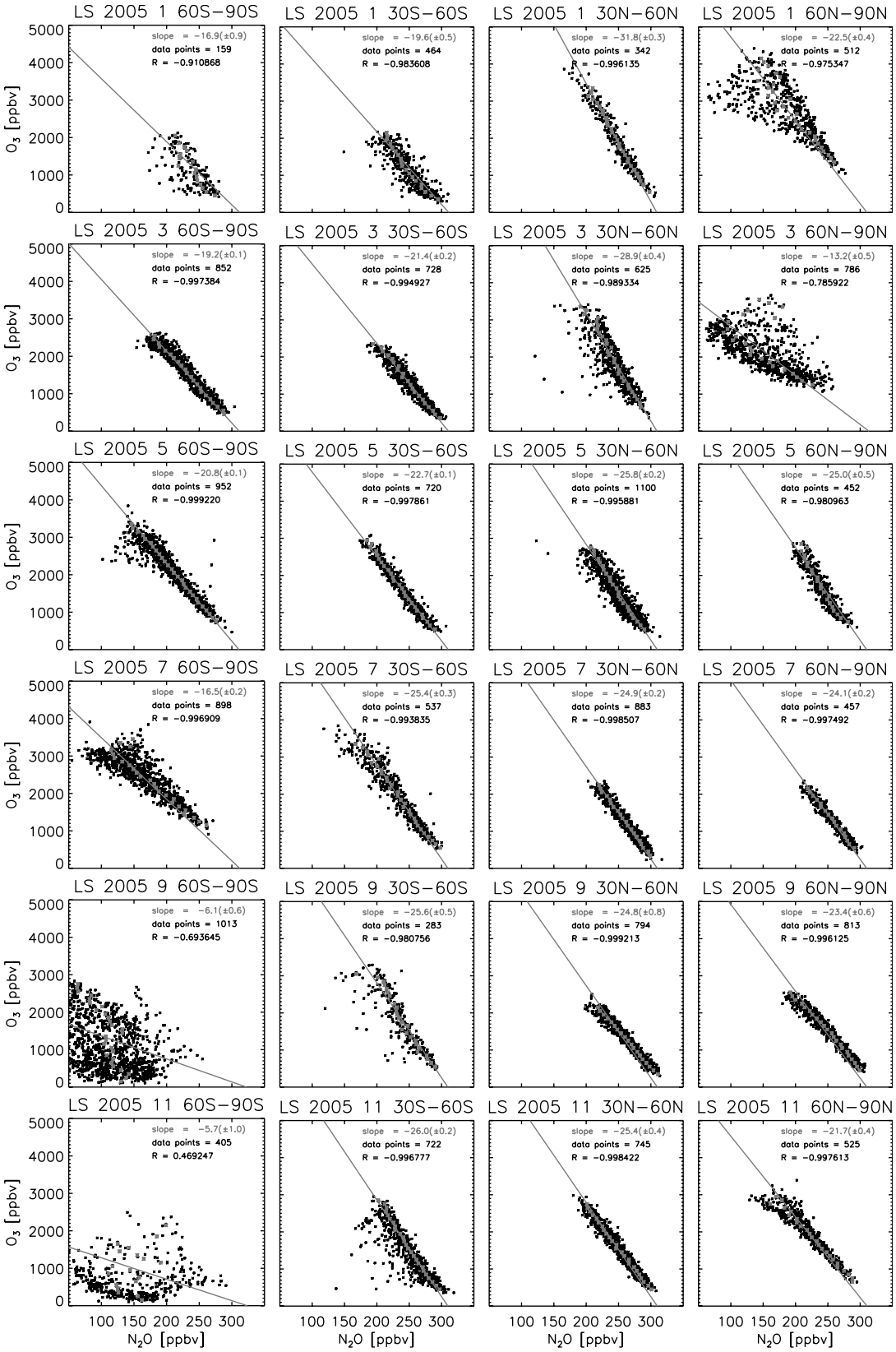

Figure 11. Monthly O_3-N_2O scatter plots from ACE in the lower stratosphere (between 400 and 500 K) for different latitude bands. Data are classified according to their equivalent latitude and shown for the year 2005 and every second month from January on. The shaded lines denote the linear fit through the median values of N_2O (shaded asterisks) obtained for O_3 bins with a width of 100 ppbv and constrained by a tropospheric endpoint.

Table 2. Absolute Slope Values ($-\Delta O_3/\Delta N_2O$) From Measurements Compiled by *Proffitt et al.* [2003] and Obtained During SPURT[a]

	$-\Delta O_3/\Delta N_2O$
Measurements NH LS Compiled by Proffitt et al. [2003]	
Feb midlatitudes (AASE 1989)	27.88
May midlatitudes (ATMOS Shuttle 1985)	27.20
Winter high latitudes (AASE II 1991–1992)	23.06
Winter high latitudes (AASE 1989)	22.42
Apr high latitudes (ATMOS Shuttle 1993)	22.02
Dec high latitudes (HALOE Satellite 1991)	23.1
SPURT Measurements NH LMS	
Nov 2001 (autumn)	27.9 ± 0.3
Jan 2002 (winter)	24.0 ± 0.4
May 2002 (spring)	19.1 ± 0.1
Aug 2002 (summer)	20.8 ± 0.5
Oct 2002 (autumn)	26.8 ± 0.2
Feb 2003 (winter)	23.7 ± 0.2
Apr 2003 (spring)	17.5 ± 0.1
Jul 2003 (summer)	18.1 ± 0.2

[a]For SPURT the standard deviations of the slopes are also provided.

figures is that the correlations are generally compact. However during winter and spring of both hemispheres, the compactness of the correlations in the polar vortex tends to be destroyed by chemical ozone loss.

[27] For reference, the ACE and CMAM correlation slopes are compared to older measurements. Table 2 provides a compilation of the correlation slopes for the different latitude bands and years from *Proffitt et al.* [2003] and the SPURT campaign. The data of the SPURT campaign are described by *Hegglin et al.* [2006]. Note that the SPURT correlation slopes have been recalculated using the procedure described here. As a consequence of forcing the linear fits toward a tropospheric value, the SPURT autumn slopes became slightly lower than the values published by *Hegglin et al.* [2006]. (For the community interested in CCM validation we provide the correlation slopes derived from the ACE measurements for the different regions, months, and years in Tables S1 and S2 in the auxiliary material.)

4.2. Testing the ACE Sampling

[28] Once again, we use CMAM to assess the representativeness of the ACE correlation slopes. We do this by comparing correlation slopes calculated from the full and subsampled CMAM data sets (Figure 12), examining the seasonal evolution of the slopes for the different regions, latitude bands, and hemispheres. The results for the full CMAM data represent a 10-year climatology and the gray and blue bars reflect the observed interannual variability. For the subsampled CMAM, each month and year is represented by its own data point, provided sufficient data points are available to define a robust correlation.

[29] Comparing full to subsampled CMAM results shows that where the midlatitude and polar slopes are the same the slopes are very well estimated by the subsampling (e.g., NH LMS). This is no surprise, since in this case the extratropics are well mixed and the correlations compact. However, where the polar and midlatitude slopes diverge, indicating the presence of a mixing barrier, there is quite a lot of scatter in the subsampled slopes (NH LS January-March, and SH LS July-October at midlatitudes). Looking at the scatterplots themselves, this is where the correlations also lose compactness. In these cases, the slopes are not particularly well represented by sparse measurements and we have to look at the picture qualitatively rather than quantitatively. (This result also has implications for studies using tracer-tracer correlations to infer chemical ozone loss.) Nevertheless we can look at the seasonal cycles to get an understanding of the combined effects of transport and chemistry in this region.

4.3. Model-Measurement Comparison

[30] Having gained confidence in the overall representativeness of the ACE data, we turn to the model-measurement comparison. In Figure 13, the full 10-year climatology of the CMAM correlation slopes is repeated from Figure 12, and is now to be compared with the correlation slopes calculated for the ACE data set. The standard deviation for the ACE slopes now includes an estimate of the measurement errors. Distinct seasonal cycles are obtained from ACE for all the different data groupings. The error bars of the linear fits are small enough to allow the seasonal cycles to be well defined, and the slopes are seen to compare well to the correlation slopes derived from the ER-2 and SPURT aircraft measurements in the NH. Larger error bars, as found in NH and SH autumn in the LMS, are primarily caused by a smaller dynamic range of the observed O_3 and N_2O mixing ratios caused by the decreasing volume (i.e., altitude range) of the LMS during this season and a weaker transport

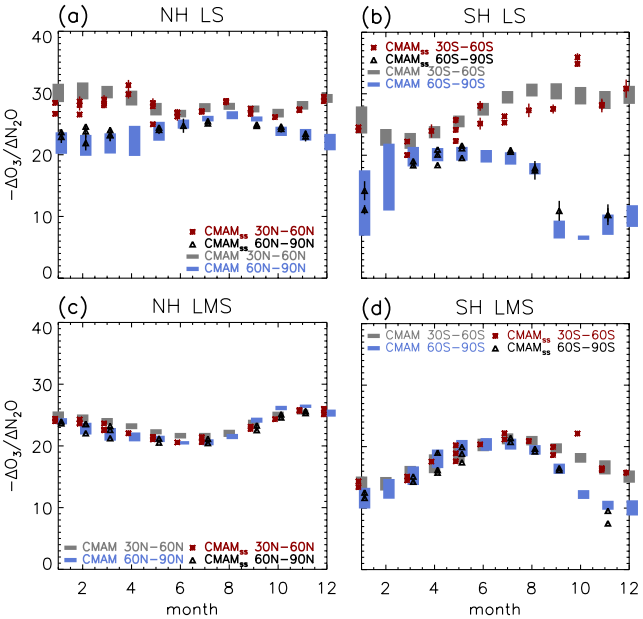

Figure 12. Negative of $\Delta O_3/\Delta N_2O$ and standard deviations in (a and b) the NH and SH LS and (c and d) the NH and SH LMS; see definitions in text. Two data sets are considered: the CMAM climatology of 10 years for midlatitudes (gray bars) and polar regions (blue bars), and CMAM data subsampled according to the ACE retrieval locations for midlatitudes (red asterisks) and polar regions (black triangles). Both data sets are classified according to their equivalent latitude into the different latitude bands.

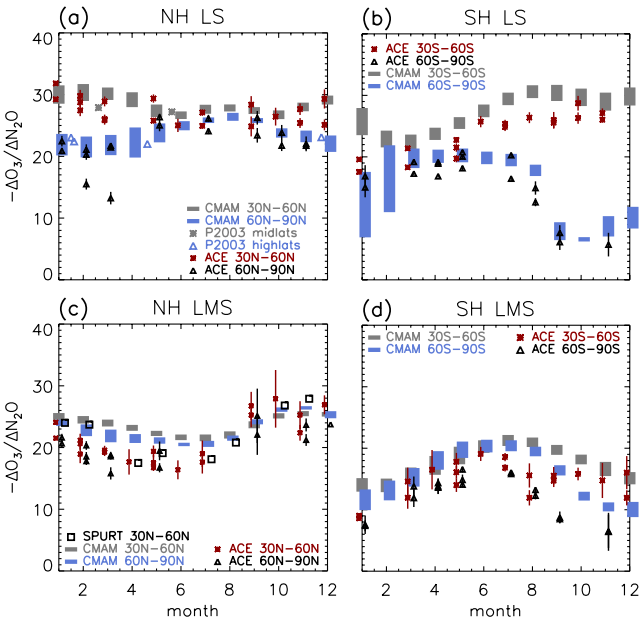

Figure 13. Same as Figure 12 but four different data sources are considered: CMAM climatology of 10 years for midlatitudes (gray bars) and polar regions (blue bars), ACE satellite data from midlatitudes (red asterisks) and polar regions (black triangles), SPURT aircraft data from midlatitudes (black squares) during 2001–2003 from *Hegglin et al.* [2006] but recalculated using the here presented method, i.e., constrained to a tropospheric endpoint, and ER-2, shuttle, or HALOE satellite data from midlatitudes (gray asterisks) and polar regions (blue triangles) compiled by *Proffitt et al.* [2003]. The in situ measurements are from separate campaigns. All data except the ER-2 measurements were classified according to their equivalent latitude into the different latitude bands.

of photochemically aged stratospheric air into the LMS (see Figure 9).

[31] We now discuss and interpret the ACE results, and their comparison with CMAM, for each hemisphere and vertical region separately. In general, the CMAM slopes are slightly larger than the ACE slopes, which may reflect the slight young bias in the CMAM age of air. The young bias is somewhat stronger in the SH than in the NH. However, because of the sensitivity of the correlation slopes to the value of the tropospheric N_2O endpoint, we primarily focus attention on the seasonal evolution and the polar-midlatitude differences of the correlation slopes, rather than on their absolute magnitude.

4.3.1. Lower Stratosphere

[32] In the NH LS (Figure 13a), the ACE slopes in midlatitudes exhibit a maximum in late winter and a minimum in late summer. The slopes in the polar region show a similar amplitude of the annual cycle, but the maximum and minimum values are shifted by six months compared with midlatitudes. CMAM produces similarly distinct and robust seasonal cycles, although the polar slopes appear to be somewhat higher than the ones obtained from ACE. The winter of 2005 produced particularly small slopes in the ACE data in the Arctic due to enhanced chemical ozone loss [cf. *Manney et al.*, 2006], which as discussed earlier are not within the range of the CMAM variability. The seasonal cycles in the midlatitude O_3-N_2O slopes reflect the poleward and downward transport of high-ozone air mainly during winter, followed by photochemical decay of the ozone values during summer. During winter the midlatitude and polar branches are distinct indicating a transport barrier, but in late spring, after the breakup of the polar vortex, the branches merge, elevating the polar values. Thus the seasonal evolution of the NH polar slopes is strongly affected by mixing with midlatitudes. By autumn the branches begin to separate again as the polar vortex develops and the Brewer-Dobson circulation strengthens. The associated decreasing slopes indicate that the polar LS is supplied with air from higher altitudes and thus with older air than in the midlatitudes. This is consistent with the distribution of age of air as seen in Figure 1.

[33] In the SH LS (Figure 13b), the seasonal evolution of the ACE slopes in midlatitudes is approximately the same as in the NH, but the minimum and maximum are shifted one or two months later. The seasonal cycle of the polar slopes is distinctly different, with the SH minimum occurring even later in spring than in the NH, and the maximum in winter. Both the amplitude of the seasonal cycles and the separation between the polar and midlatitude branches are much greater in the SH than in the NH. The CMAM slopes are generally in good agreement with the ACE slopes. Chemistry evidently plays a much greater role in determining the seasonal cycles of the correlation slopes in the SH, with the polar values lowering the midlatitude values in summer after the breakup of the polar vortex. This is analogous to the effect of Antarctic ozone loss on the SH midlatitude summertime ozone trend [*Fioletov and Shepherd*, 2005, Figure 4 (top)]. The period of time when the polar and midlatitude branches are merged is much shorter than in the NH because of the longer "dynamical winter" and the stronger chemical influence in the SH.

4.3.2. Lowermost Stratosphere

[34] In the NH LMS (Figure 13c), the ACE slopes in both the polar and midlatitude regions exhibit an autumn maximum and spring minimum, as noted by *Hegglin et al.* [2006] on the basis of SPURT aircraft measurements. Furthermore the polar and midlatitude behaviors are very similar. The seasonalities seen here are thus distinctly different from the seasonalities seen in the NH LS. *Hegglin et al.* [2006] interpreted the seasonal cycle of the O_3-N_2O correlation in the LMS as being due to a change in air mass origin, with a "flushing" of the LMS with younger tropical air masses via the tropically controlled transition region during autumn as the mass flux across the 380 K isentrope strengthens. Here the CMAM slopes show a similar evolution of the slopes as seen in the observations, but the amplitude of the seasonal cycle is too weak compared to both SPURT and ACE. Because the tropical lower stratosphere has a distinct correlation branch with very high slopes (and young air), excessive mixing and transport in the tropically controlled transition region and into the LMS, as can be expected in CMAM because of limited horizontal resolution, will tend to increase the slopes and/or dampen the annual cycle.

[35] In the SH LMS (Figure 13d), the ACE slopes are reminiscent of the SH LS, showing a strong impact of polar

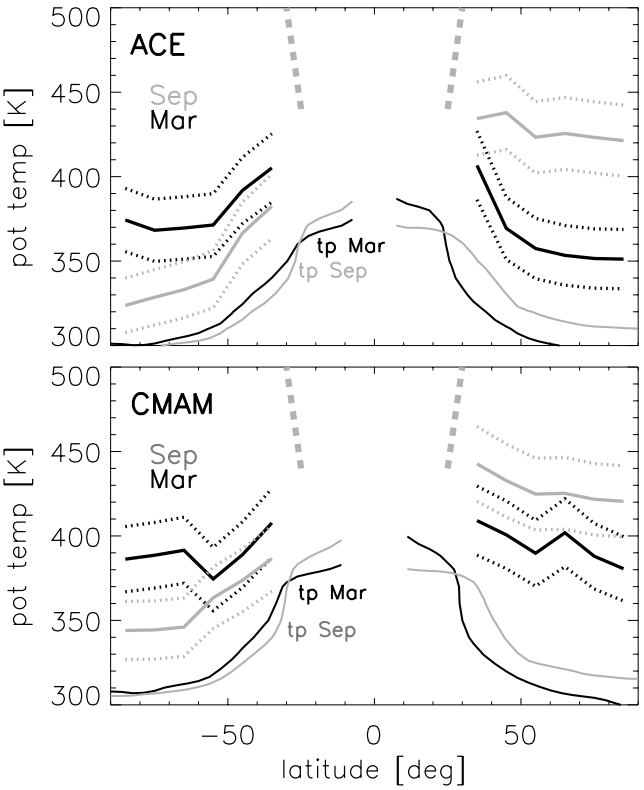

Figure 14. Potential temperature values where the LS and LMS correlation slopes intersect, as a function of latitude, for (top) ACE and (bottom) CMAM. The values (thick solid lines) and their estimated 5% uncertainties (dotted lines, including sensitivity to tropospheric endpoint value in the LS slope) are shown for September (gray) and March (black). Also indicated are approximate locations of the tropical pipe (dashed gray line) and, in both panels, the CMAM dynamical tropopause for September and March (gray and black thin lines, respectively).

ozone chemistry. The maximum in the slopes is seen in winter and the minimum in spring, whereas the separation of the polar and the midlatitude branches does not begin until September, merging again in late summer. CMAM is in reasonable agreement with the observations regarding the seasonal evolution of the slopes and the separation between the midlatitude and polar branches. The deficiencies seen in the NH LMS are apparently overwhelmed in the SH LMS by the chemical control of the seasonal cycle through the influence of polar ozone loss.

4.3.3. "Flushing" of the Lowermost Stratosphere

[36] The classification of the data into LS and LMS air masses considered above is somewhat arbitrary. However, we can determine the potential temperature level at which the derived correlation slopes intersect, which presents a more natural division between the two air masses based on their chemical characteristics. This provides an alternative (and more physical) way of looking at the seasonal dependence of the correlation slopes shown in Figure 13. The results are given in Figure 14 for both ACE and CMAM, as a function of latitude. The ACE data indicate that this "chemically defined" LMS is confined to a few km above the tropopause (roughly 50 K) in spring, but extends to much higher altitudes in autumn. (Note that the extratropical transition layer (ExTL) exhibiting substantial tropospheric influence is only the lowest part of this "chemically defined" LMS, and is no more than around 2 km thick [e.g., *Hoor et al.*, 2004]. As noted earlier, the ExTL corresponds to endpoint mixing and is not expected to be visible in the O_3-N_2O correlations.) This seasonality reflects the strong influence of downwelling from the Brewer-Dobson circulation in winter and spring, which brings older stratospheric air to lower altitudes, and the "flushing" of the region with younger air via the tropically controlled transition region toward autumn. This is most evident in the NH, where it is notable that the "chemically defined" LMS encompasses the tropical transition region in autumn, reaching up to the bottom of the tropical pipe. Both the Brewer-Dobson downwelling and the latitudinal mixing are weaker in the SH, and there is furthermore a dominating chemical control on the seasonal evolution of the correlation slopes. Note that the strong latitudinal dependence of the intersection level in spring, but not in autumn, is consistent with the differences between the polar and midlatitude correlation slopes in Figure 13.

[37] The intersection levels derived from CMAM generally reflect the behavior seen in the ACE data, although in NH spring the "chemically defined" LMS is too deep. This supports the interpretation of too strong mixing from the tropical lower stratosphere in CMAM during this period.

5. Summary and Discussion

[38] In this study, we examined the stratospheric O_3-N_2O correlation structure using measurements from the Atmospheric Chemistry Experiment Fourier Transform Spectrometer (ACE-FTS) satellite instrument, reaching into the tropopause region with a vertical resolution down to 1 km, thereby extending the spatial and temporal coverage provided by earlier (mainly aircraft) measurements. The results have been interpreted in a geophysical context and the potential of the O_3-N_2O correlation as a process-oriented validation diagnostic for chemistry-climate models (CCMs) has been revisited. When comparing models and measurements, care must be taken that the chosen diagnostic is robust to sampling uncertainties or biases. To assess the representativeness of the ACE measurements, which are quite sparse, as ACE is a solar occultation instrument, we use the Canadian Middle Atmosphere Model (CMAM), a comprehensive CCM, by subsampling the full CMAM fields according to the ACE retrieval locations and comparing them to the full data fields in the context of a given diagnostic.

[39] In the middle stratosphere, where the O_3-N_2O correlations are not compact, the fan-shaped structure of the overall correlation pattern in both hemispheres reflects the gross effects of the Brewer-Dobson circulation together with the chemical sources and sinks of the two species. While there is some evidence of a clustering of ACE O_3-N_2O pairs, this is shown to be at least partly an artifact of the limited ACE sampling. A way of avoiding sampling biases and allowing a meaningful comparison with models is to compute equal-area joint (two-dimensional) PDFs. This also obviates the need to use equivalent latitude, as structures reflecting transport and mixing emerge naturally. In order to

avoid gaps in the latitudinal coverage, we use seasonally accumulated ACE data. We then calculated PDFs of O_3-N_2O for the CMAM, which has homogeneous spatiotemporal coverage. The comparison of the joint PDF of the subsampled CMAM data to that of the full CMAM data shows that the dynamical features in the ACE observations which are revealed by this method can be trusted. The CMAM PDFs highlight many detailed features of transport and mixing and their seasonal evolution, such as the stratospheric surf zone and the subtropical and polar vortex edges, which are also reflected in the somewhat noisier ACE PDFs. The comparison, however, reveals that CMAM lacks a signature of the tropical pipe in NH MAM and JJA. This comparison indicates the potential value of the joint PDF diagnostic for process-oriented model validation in a region of the stratosphere where the O_3-N_2O correlations are not compact, hence presenting an alternative diagnostic to the one suggested by *Proffitt et al.* [2003].

[40] Below about 21 km, the ACE data generally confirm the compactness of the O_3-N_2O correlation as found in previous aircraft, balloon, and shuttle measurements, and reveal distinct polar and midlatitude branches in this region, particularly in the SH. However, strong chemical ozone loss tends to destroy the compactness, and the slopes in such cases are to be interpreted in a qualitative rather than a quantitative manner. Furthermore, the calculation of the correlation slopes is sensitive to the choice of the tropospheric endpoint value, especially in the LS where the endpoint does not correspond to the average tropospheric O_3 and N_2O mixing ratios and is not well defined. We hence compare the polar and midlatitude branches derived from the measurements and the CMAM by focusing on the seasonal evolution of the correlation slopes in these two latitude bands in two different altitude ranges, referred to as the lower stratosphere (LS), approximately 16–21 km, and the lowermost stratosphere (LMS), from the tropopause up to 16 km. This extends the analysis of *Proffitt et al.* [2003] in the NH midlatitude and polar LS, and *Hegglin et al.* [2006] in the NH midlatitude LMS using SPURT aircraft measurements. In the NH, the seasonal evolution of the observed correlation slopes is mainly controlled by transport and mixing, and is very different in the LS and LMS, revealing the different balances between diabatic descent and horizontal mixing in these two regions. CMAM also exhibits distinctly different behavior in the LS and LMS, and the seasonal evolution of its correlation slopes agrees quite well with the observations in both regions. However, CMAM underestimates the variability in Arctic polar ozone loss, and also the amplitude of the seasonal cycle in the NH LMS. The latter behavior is attributed to excessive horizontal mixing within the tropically controlled transition region, which is possibly due to a too low horizontal resolution affecting the breaking of synoptic-scale waves in this region, the latter being ultimately responsible for the horizontal mixing between the tropics and the midlatitudes. In the SH, the seasonal evolution of the observed correlation slopes is strongly affected by the ozone hole, which leads to a large separation between the polar and midlatitude slopes throughout most of the year, and to very similar behavior in the LS and LMS. Because of this strong chemical control, CMAM is able to follow the observations quite well. A "chemically defined" LMS can be derived from the potential temperature level at which the LMS and LS correlation slopes intersect. This diagnostic reveals in a clear physical way the "flushing" of the extratropical region with younger air from the tropical lower stratosphere between spring and autumn, especially in the NH where the region of influence extends up to the bottom of the tropical pipe, around 430 K. In spring, on the other hand, this "chemically defined" LMS is generally below 350 K. These levels contrast with the traditional definition of the LMS as being below 380 K (the level of the tropical tropopause).

[41] **Acknowledgments.** We thank the ACE science team, Peter Bernath, Sean McLeod, Chris Boone, Kaley Walker, and Ian Folkins for providing the ACE data and Gloria Manney for the derived meteorological products. Thanks to David Sankey for providing the CMAM data. ACE is funded primarily by the Canadian Space Agency. This research has been supported by the Canadian Foundation for Climate and Atmospheric Sciences and the Canadian Space Agency through the C-SPARC program. We are grateful for helpful comments from the reviewers of this and an earlier version of the manuscript and for helpful discussions with Jessica Neu and Charles McLandress.

References

Austin, J., et al. (2003), Uncertainties and assessments of chemistry-climate models of the stratosphere, *Atmos. Chem. Phys.*, *3*, 1–27.

Beagley, S. R., J. de Grandpré, J. N. Koshyk, N. A. McFarlane, and T. G. Shepherd (1997), Radiative-dynamical climatology of the first-generation Canadian Middle Atmosphere Model, *Atmos. Ocean*, *35*, 293–331.

Bernath, P. F., et al. (2005), Atmospheric Chemistry Experiment (ACE): Mission overview, *Geophys. Res. Lett.*, *32*, L15S01, doi:10.1029/2005GL022386.

Boering, K. A., S. C. Wofsy, B. C. Daube, J. R. Schneider, M. Loewenstein, J. R. Podolske, and T. J. Conway (1996), Stratospheric mean ages and transport rates from observations of CO_2 and N_2O, *Science*, *274*, 1340–1343.

Boone, C. D., et al. (2005), Retrievals for the Atmospheric Chemistry Experiment Fourier Transform Spectrometer, *Appl. Opt.*, *44*, 7218–7231.

Bregman, A., J. Lelieveld, M. M. P. van den Broek, P. C. Siegmund, H. Fischer, and O. Bujok (2000), N_2O and O_3 relationship in the lowermost stratosphere: A diagnostic for mixing processes as represented by a three-dimensional chemistry-transport model, *J. Geophys. Res.*, *105*, 17,279–17,290.

de Grandpré, J., S. R. Beagley, V. I. Fomichev, E. Griffioen, J. C. McConnell, A. S. Medvedev, and T. G. Shepherd (2000), Ozone climatology using interactive chemistry: Results from the Canadian Middle Atmosphere Model, *J. Geophys. Res.*, *105*, 26,475–26,491.

Eyring, V., et al. (2006), Assessment of temperature, trace species and ozone in chemistry-climate model simulations of the recent past, *J. Geophys. Res.*, *111*, D22308, doi:10.1029/2006JD007327.

Eyring, V., et al. (2007), Multimodel projections of stratospheric ozone in the 21st century, *J. Geophys. Res.*, *112*, D16303 doi:10.1029/2006JD008332.

Fioletov, V. E., and T. G. Shepherd (2005), Summertime total ozone variations over middle and polar latitudes, *Geophys. Res. Lett.*, *32*, L04807, doi:10.1029/2004GL022080.

Fussen, D., F. Vanhellemont, J. Dodion, C. Bingen, K. A. Walker, C. D. Boone, S. D. McLeod, and P. F. Bernath (2005), Initial intercomparison of ozone and nitrogen dioxide number density profiles retrieved by the ACE-FTS and GOMOS occultation experiments, *Geophys. Res. Lett.*, *32*, L16S02, doi:10.1029/2005GL022468.

Hegglin, M. I., et al. (2006), Measurements of NO, NO_y, N_2O, and O_3 during SPURT: Implications for transport and chemistry in the lowermost stratosphere, *Atmos. Chem. Phys.*, *6*, 1331–1350, sref:1680-7324/acp/2006-6-1331.

Hoor, P., C. Gurk, D. Brunner, M. I. Hegglin, H. Wernli, and H. Fischer (2004), Seasonality and extent of extratropical TST derived from in-situ CO measurements during SPURT, *Atmos. Chem. Phys.*, *4*, 1427–1442.

Intergovernmental Panel on Climate Change (2000), *Special Report on Emissions Scenarios: A Special Report of Working Group III of the Intergovernmental Panel on Climate Change*, 599 pp., Cambridge Univ. Press, Cambridge, U. K.

Khosrawi, F., R. Müller, M. H. Proffitt, and H. Nakajima (2004), Monthly averaged ozone and nitrous oxide from the Improved Limb Atmospheric Spectrometer (ILAS) in the Northern and Southern Hemisphere polar regions, *J. Geophys. Res.*, *109*, D10301, doi:10.1029/2003JD004365.

Khosrawi, F., R. Müller, M. H. Proffitt, and H. Nakajima (2006), Monthly averages of nitrous oxide and ozone for the Northern and Southern high latitudes: A "1-year climatology" derived from ILAS/ILAS-II observations, *J. Geophys. Res.*, *111*, D11S11, doi:10.1029/2005JD006384.

Logan, J. A. (1999), An analysis of ozonesonde data for the lower stratosphere: Recommendations for testing models, *J. Geophys. Res.*, *104*, 16,151–16,170.

Manney, G. L., M. L. Santee, L. Froidevaux, K. Hoppel, N. J. Livesey, and J. W. Waters (2006), EOS MLS observations of ozone loss in the 2004–2005 Arctic winter, *Geophys. Res. Lett.*, *33*, L04802, doi:10.1029/2005GL024494.

Michelsen, H. A., G. L. Manney, M. R. Gunson, and R. Zander (1998), Correlations of stratospheric abundances of NO_y, O_3, N_2O, and CH_4 derived from ATMOS measurements, *J. Geophys. Res.*, *103*, 28,347–28,359.

Müller, R., U. Schmidt, A. Engel, D. S. McKenna, and M. H. Proffitt (2001), The O_3-N_2O relation from balloon-borne observations as a measure of Arctic ozone loss in 1991/92, *Q. J. R. Meteorol. Soc.*, *127*, 1389–1412.

Müller, R., et al. (2003), Chlorine activation and chemical ozone loss deduced from HALOE and balloon measurements in the Arctic during the winter of 1999–2000, *J. Geophys. Res.*, *107*, 8302, doi:10.1029/2001JD001423 [printed *108*(D5), 2003].

Murphy, D. M., and D. W. Fahey (1994), An estimate of the flux of stratospheric reactive nitrogen and ozone into the troposphere, *J. Geophys. Res.*, *99*, 5325–5332.

Neu, J. L., L. C. Sparling, and R. A. Plumb (2003), Variability of the subtropical "edges" in the stratosphere, *J. Geophys. Res.*, *108*(D15), 4482, doi:10.1029/2002JD002706.

O'Sullivan, D., and P. Chen (1996), Modeling the quasi biennial oscillation's influence on isentropic tracer transport in the subtropics, *J. Geophys. Res.*, *101*, 6811–6821.

Plumb, R. A., and M. K. W. Ko (1992), Interrelationships between mixing ratios of long-lived stratospheric constituents, *J. Geophys. Res.*, *97*, 10,145–10,156.

Proffitt, M. H., D. W. Fahey, K. K. Kelly, and A. F. Tuck (1989), High-latitude ozone loss outside the Antarctic ozone hole, *Nature*, *342*, 233–237.

Proffitt, M. H., J. J. Margitan, K. K. Kelly, M. Loewenstein, J. R. Podolske, and K. R. Chan (1990), Ozone loss in the Arctic polar vortex inferred from high-altitude aircraft measurements, *Nature*, *347*, 31–36.

Proffitt, M. H., K. Aikin, J. J. Margitan, M. Loewenstein, J. R. Podolske, A. Weaver, K. R. Chan, H. Fast, and J. W. Elkins (1993), Ozone loss inside the northern polar vortex during the 1991–1992 winter, *Science*, *261*, 1150–1154.

Proffitt, M. H., K. Aikin, J. J. Margitan, C. R. Webster, G. C. Toon, and J. W. Elkins (2003), Seasonally averaged ozone and nitrous oxide in the Northern Hemisphere lower stratosphere, *J. Geophys. Res.*, *108*(D3), 4110, doi:10.1029/2002JD002657.

Rosenlof, K., A. F. Tuck, K. K. Kelly, J. M. Russell, and M. P. McCormick (1997), Hemispheric asymmetries in water vapor and inferences about transport in the lower stratosphere, *J. Geophys. Res.*, *102*, 13,213–13,234.

Sankey, D., and T. G. Shepherd (2003), Correlations of long-lived chemical species in a middle atmosphere general circulation model, *J. Geophys. Res.*, *108*(D16), 4494, doi:10.1029/2002JD002799.

Sparling, L. C. (2000), Statistical perspectives on stratospheric transport, *Rev. Geophys.*, *38*, 417–436.

Strahan, S. E. (1999), Climatologies of lower stratospheric NO_y and O_3 and correlations with N_2O based on in situ observations, *J. Geophys. Res.*, *104*(D23), 30,463–30,480.

Tegtmeier, S., and T. G. Shepherd (2007), Persistence and photochemical decay of springtime total ozone anomalies in the Canadian Middle Atmosphere Model, *Atmos. Chem. Phys.*, *7*, 485–493.

Tilmes, S., R. Müller, J.-U. Grooss, H. Nakajima, and Y. Sasano (2006), Development of tracer relations and chemical ozone loss during the setup phase of the polar vortex, *J. Geophys. Res.*, *111*, D24S90, doi:10.1029/2005JD006726.

Volk, M. C., et al. (1996), Quantifying transport between the tropical and mid-latitude lower stratosphere, *Science*, *21*, 1763–1768.

Walker, K. A., C. E. Randall, C. R. Trepte, C. D. Boone, and P. F. Bernath (2005), Initial validation comparisons for the Atmospheric Chemistry Experiment (ACE-FTS), *Geophys. Res. Lett.*, *32*, L16S04, doi:10.1029/2005GL022388.

Waugh, D., et al. (1997), Mixing of polar vortex air into middle latitudes as revealed by tracer-tracer scatterplots, *J. Geophys. Res.*, *102*, 13,119–13,134.

World Meteorological Organization (2003), Scientific assessment of ozone depletion: 2002, *Global Ozone Res. and Monit. Proj., Rep. 47*, World Meteorol. Organ., Geneva, Switzerland.

M. I. Hegglin and T. G. Shepherd, Department of Physics, University of Toronto, 60 St. George Street, Toronto, ON, Canada M5S 1A7. (michaela@atmosp.physics.utoronto.ca; tgs@atmosp.physics.utoronto.ca)